Spin-Polarized Transport in Carbon Nanowires Inside Semiconducting Carbon Nanotubes

ARTICLE *in* THE JOURNAL OF PHYSICAL CHEMISTRY C · JUNE 2007

Impact Factor: 4.77 · DOI: 10.1021/jp073320e

Spin-Polarized Transport in Carbon Nanowires Inside Semiconducting Carbon Nanotubes

X. Q. Shi, Z. X. Dai, G. H. Zhong, X. H. Zheng, and Z. Zeng*

Key Laboratory of Materials Physics, Institute of Solid State Physics, Chinese Academy of Sciences, Hefei 230031, China and Graduate School of the Chinese Academy of Sciences, Beijing 100049

Received: April 30, 2007

A first-principles approach combined with none-equilibrium Green's function method is used to investigate the spin-polarized transport properties of a kind of all-carbon composite: carbon nanowires (CNW) in the core of single-walled carbon nanotubes. Our results indicate that if the CNW density is not too high, spin-polarized transmission spectra are obtained resulting from the two majority spin bands induced near the Fermi level. With the bias voltages applied, spin-polarized current and negative differential resistance (NDR) appear. The appearance of NDR can be analyzed from the mismatch of the energy bands in the left and right leads due to external bias voltages. Other factors that influence the degree of spin-polarization are also discussed.

1. Introduction

Molecular electronics has attracted increasing interests both for the fundamental reasons and for the potential applications since it represents the ultimate miniaturization of electronic systems.[1] In such an active research field, some important factors for electronics applications have been proven at the molecular level, such as negative differential resistance (NDR)[2] and rectification.[3] Moreover, molecular transistors, memories, and logic gates have also been demonstrated.[4] Since the pioneering work of Tsukagoshi and co-workers,[5] in which spin-polarized electrons are injected into carbon nanotubes, a new field, molecular spintronics,[6] appears. Molecular spintronics is the integration of molecular electronics and spintronics.[7] A growing activity in this burgeoning area has been stimulated and good tunnel magnetoresistance (TMR) characteristics have already been measured in octanethiols[8] and polymers.[9]

The carbon nanotubes (CNTs), which are promising materials for future nanoscale electronic devices,[10] have drawn much attention since their discovery.[11] Especially, TMR-like transport through carbon nanotubes has been experimentally reported by several groups.[5,12] The rich science of CNTs has been further enriched by two recent experimental observations of a kind of all-carbon composite, which are formed by one-dimensional carbon nanowires (CNWs) inserted into the innermost tube of multiwalled CNTs.[13] Theoretically, several groups have investigated the energetic, electronic, and magnetic properties of CNWs inserted into single-walled carbon nanotubes (referred to as CNW@SWNT in the following).[14−16] Especially, Yang et al. have studied the magnetic properties of the CNW@SWNT composites. They have found that if the CNW density is not too high (i.e., the interatomic distance of CNW is long enough), the flatband ferromagnetism will be found in the composite, which is caused by the weak coupling between the CNW and the SWNT shell.[15] At the same time, the magnetic properties of CNTs have also been probed by other authors.[17] However, to the best of our knowledge, the spin-polarized transport properties of the pure carbon composite CNW@SWNT has not been reported yet.

In the present work, we present theoretical investigations on the transport properties of the pure carbon composites, which are assumed to be composed of CNW inserted into the core of SWNTs or a single carbon atom in SWNTs. The calculated results show that as long as the CNW density is not too high spin-polarized transmission spectra can be obtained resulting from two majority spin bands induced near the Fermi level. These results agree well with previous works[15,16] about the electronic structure calculations of this kind of all-carbon composite.

This paper is organized in the following way: the computational method and the simulation model are briefly described in section II, the results and discussions are presented in section III, and a short summary is given in section IV.

2. Calculation Method and Simulation Model

Our theoretical calculations are performed with the program Atomistix ToolKit,[18] in which the density functional theory is combined with Keldysh none-equilibrium Green's function method to calculate the electronic and transport properties of nanoscale systems. The whole system, as shown in Figure 1, is divided into three parts from left to right in practical theoretical simulations: the left lead, the central scattering region, and the right lead. The interaction of the semi-infinite left and right leads on the scattering region is taken into account through self-energies. Details of the method and relevant references can be found elsewhere.[18] The bias voltage V_b is applied across the nanotube device, which drives a steady-state current to flow along the tube axis. The V_b provides the natural electrostatic boundary conditions for the Hartree potential in the scattering region, which is self-consistently solved on a three-dimensional real space grid.[18] The transmission coefficient $\mathcal{T}_{\uparrow(\downarrow)}(E,V_b)$, which is a function of energy E and V_b, is calculated from Green's functions,[18,19] and the electrical current is obtained via the Landauer−Büttiker formula

$$I_{\uparrow(\downarrow)} = \frac{e}{h}\int_{-\infty}^{+\infty} \mathcal{T}_{\uparrow(\downarrow)}(E,V_b)[f_l(E) - f_r(E)]\,dE$$

where $f_{l,r}(E) = 1/(1 + e^{(E-\mu_{l,r})/k_BT})$ is the Fermi distribution function of the left and right lead, respectively, and $\mu_{l,r}$ is the

* Corresponding author. E-mail: zzeng@theory.issp.ac.cn.

10.1021/jp073320e CCC: $37.00
Published on Web 06/15/2007

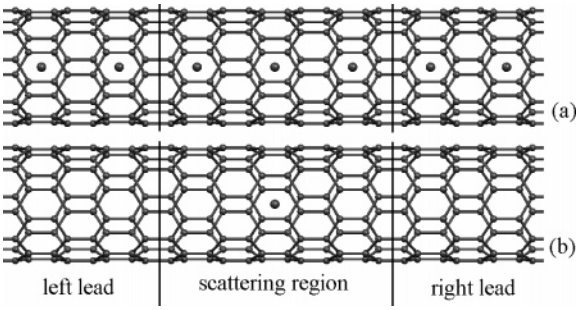

Figure 1. (a) CNW inserted into the core of (8, 0) SWNT; the CNW period is the same as that of the (8, 0) tube. (b) A single carbon atom in the tube. In practical theoretical simulations, the whole system is divided into three parts: the left lead, the scattering region, and the right lead.

electrochemical potential. Note that, in this expression, the contributions from spin-up (↑) and spin-down (↓) electrons have been explicitly separated. At zero temperature, it is written as

$$I_{\uparrow(\downarrow)} = \frac{e}{h}\int_{\mu_l}^{\mu_r} \mathcal{T}_{\uparrow(\downarrow)}(E,V_b)\,dE \quad (1)$$

Within the coherent transport regime, the effect of temperature is only induced via the lead Fermi distribution functions $f_{l,r}$. The current at finite temperature is separated into two components,[23] the "tunneling" component I_{tun} and the "thermionic emission" component I_{th} as follows:

$$I = I_{tun} + I_{th} = \frac{e}{h}[\int_{\mu_l}^{\mu_r} + (\int_{-\infty}^{\mu_l} + \int_{\mu_r}^{+\infty})]\,\mathcal{T}(E,V_b)[f_l(E) - f_r(E)]\,dE \quad (2)$$

For simplicity, we have omitted the spin label ↑(↓) in this equation.

In the calculation, the local spin density approximation in the form of the Perdew and Zunger[20] exchange-correlation functional is used. Only valence electrons are self-consistently calculated, and the atomic cores are described by standard norm conserving pseudopotential.[21] The valence wave functions are expanded by the localized numerical (pseudo)atom orbitals.[22] The *k*-point sampling is 1, 1, and 100 in the *x*, *y*, and *z* direction, which has been proven to be enough to give the converged results. The convergence criterion for the Hamiltonian, charge density, and band-structure energy is 10^{-4} via the mixture of the Hamiltonian. The positions of CNWs in the tube are relaxed until the force tolerance 0.05 eV/Å is achieved.

Figure 1 shows the typical structure used in this work, in which CNWs or a single C atom is placed in the core of the SWNT. The different CNW periods (1 and 0.5 times the period of the pure (8, 0) and (5, 5) tube) and the dimerization of the CNW are considered. The device scattering region consists of three unit cells for CNW@SWNT(8, 0), which contains 12 carbon rings with 99 atoms in all. We have checked that scattering regions containing 12 carbon rings (99 atoms) and 16 carbon rings (132 atoms) give the same transmission spectra. The electron transport direction along the tube axis is the *z* direction, and the other two vertical directions are the *x* and *y* directions. We choose a supercell with a large enough vacuum layer in the *x* and *y* directions so that the device has no interaction with its mirror images.

3. Results and Discussions

In the following, we take the geometry model shown in Figure 1 as an example to illustrate the spin-polarized transport properties of the CNW@SWNT composite. Then we also notice that there exist spin-polarized transport behaviors in other geometries only if the CNW density in these structures is not too high.

Figure 2 shows the calculated density of states (DOS), band structures, and transmission spectra ($\mathcal{T}$) of CNW@SWNT(8, 0). The most interesting is the appearance of two flatbands near the Fermi level in the original band gap of the pure (8, 0) tube, as presented by the two marked lines of Figure 2d. Specifically, these two bands are only for the spin-up electrons. Therefore, they are completely spin polarized, making the composite a ferromagnetic material. This is also clearly seen from the total DOS of CNW@SWNT(8, 0), as displayed in Figure 2a. Figure 2b,c illustrates the corresponding DOS contribution from the SWNT and the CNW, respectively. The DOS around E_F from −0.29 eV to 0.16 eV is mainly contributed from the CNW, which is identified by comparing Figure 2b,c. In the spin-up part of Figure 2d, the band with symbol □ is doubly degenerate, which is primarily composed of p_x and p_y electrons of CNW, whereas the band with symbol ○ is nondegenerate (p_z of CNW). It is these two flat spin-up bands that lead to the pure spin-up transmission around E_F. Figure 2e plots the equilibrium transmission spectra $\mathcal{T}(E,V_b = 0)$ versus incident electron energy, which obviously demonstrates that there only exists the spin-up transmission around E_F. Comparing Figure 2d,e, we observed that the fully spin-polarized transmission near E_F directly results from these two spin-up flatbands.

Since there only exists the spin-up current at lower bias voltages V_b, as presented in Figure 3a, we then focus on the spin-up bands and the corresponding transmission spectra. Figure 3b,c exemplifies the correlation between the band structure and the transmission spectra at equilibrium. It can be observed that the variations of $\mathcal{T}(E,V_b = 0)$ correlate perfectly with the band structure. The transmission spectra vary in steps of one or two because the bands are either singly or doubly degenerate. As mentioned above, these two flatbands near E_F are composed of one doubly degenerate band and one nondegenerate band. These bands results in $\mathcal{T} = 3$ below E_F and $\mathcal{T} = 1$ above E_F, because the degenerate flatband only exists below E_F. The band extending from $E = 0.17$ eV to higher energy is the "hybrid band" coming from $\sigma^*-\pi^*$ hybridization of graphitic states due to the nanotube curvature.[24] Such a hybrid band leads to the transmission of one unit; see Figure 3b,c. At even higher energy, the two degenerate antibonding π^* bands contribute to the transmission, and thus, $\mathcal{T}$ increases in step of two units.

As V_b is 0.2 V, the electrochemical potential in the left lead μ_l is shifted down by 0.1 eV, and that in the right lead μ_r is shifted up by 0.1 eV; hence, the bands in the two leads are shifted correspondingly.[25] In Figure 3d,e, the shifted electrochemical potential is denoted by the thin horizontal line. As a result of the relative shift between the bands in the left and right leads under bias, the mismatch of these bands happens; that is, only parts of the bands in the left lead match with those in the right lead because of the applied bias voltage. The matching part between the doubly degenerate flatband is denoted by symbol □, and the matching part between the nondegenerate flatband is denoted by symbol ○. These two matching parts contribute to the transmission from −0.19 eV to 0.07 eV. In the energy region from 0.07 eV to 0.26 eV, the nondegenerate flatband matches with the hybrid band, as denoted by symbol △, and then contributes to the transmission in this energy region. The matching part of the hybrid band itself, labeled as symbol ●, and that of the π^* band itself, labeled as symbol ■, are also

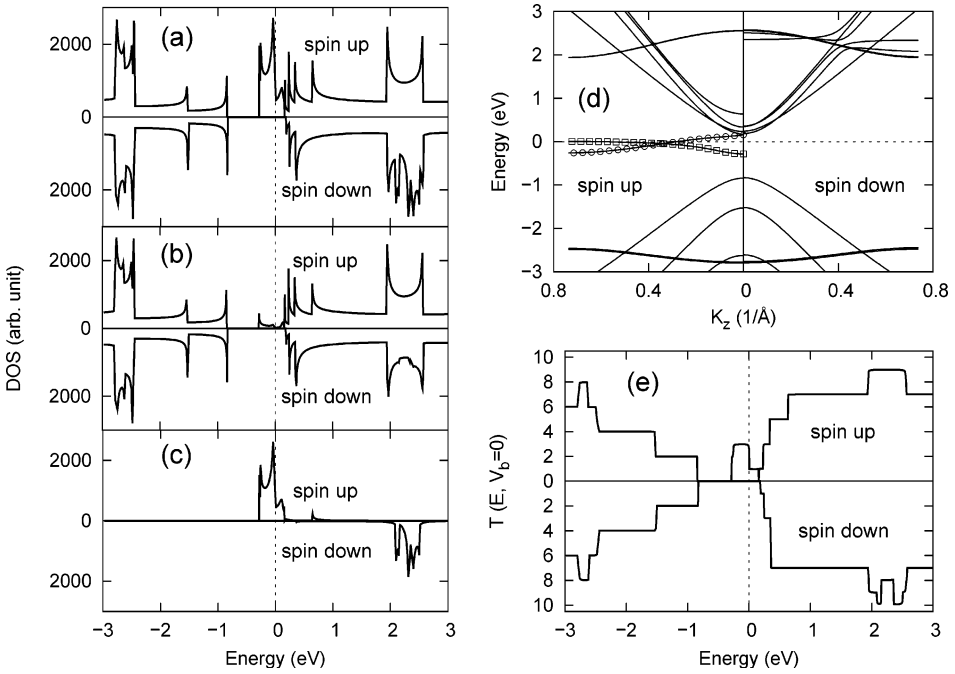

Figure 2. Obtained DOS, band structures, and transmission spectra of CNW@SWNT(8, 0): (a) total DOS, (b) DOS contribution from the tube, (c) DOS contribution from the CNW, (d) band structures, and (e) transmission spectra at equilibrium. In the spin-up part of panel d, the two bands marked with symbols □ and ○ are mainly contributed from the CNW. The Fermi level is shifted to $E_F = 0$, shown by the dashed line.

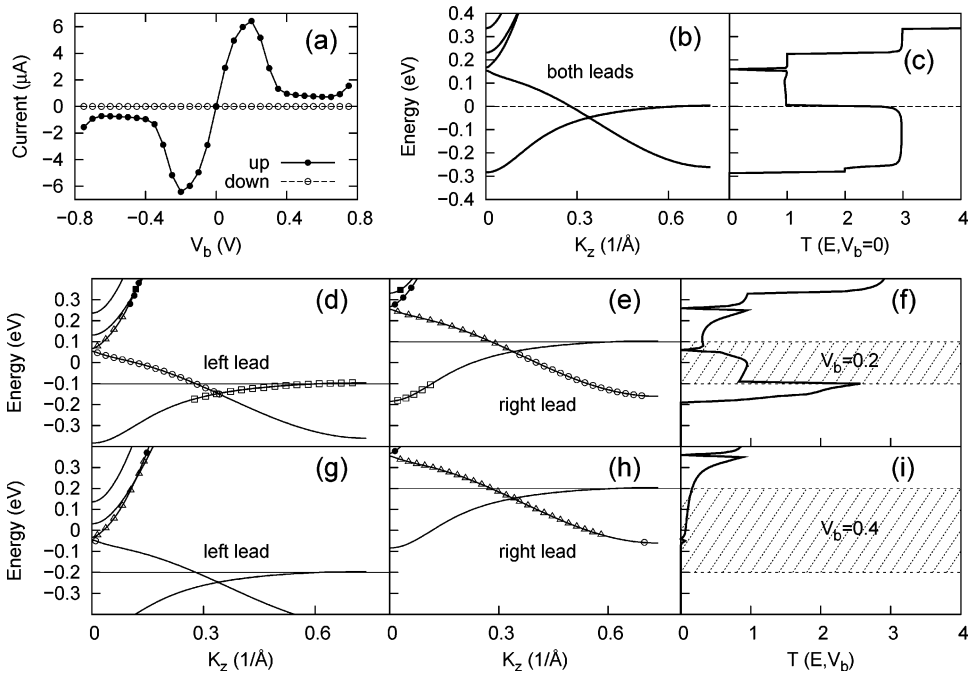

Figure 3. Electrical current, spin-up energy bands, and the corresponding spin-up transmission spectra under various biases for CNW@SWNT(8, 0). (a) The current−voltage curves for spin-up and spin-down. (b) The band structure of the leads and (c) the corresponding transmission spectra at equilibrium. (d,g) Evolution of the band structure with increasing bias voltages in the left lead and (e,h) for the right lead. (f,i) The evolution of the transmission spectra under bias voltages. The positive bias voltages shift down the electrochemical potential, and bands in the left lead and those in the right lead are shifted up. For d, e, g, and h, the shifted electrochemical potential is shown by the thin horizontal line. The bands contributing to the transmission are marked by symbols □, ○, △, ●, and ■. For f and i, the shaded energy region is the integral window.

shown. Figure 3f presents the transmission spectra with the bias being 0.2 eV. Therefore, from Figure 3d−f, we can clearly observe that the match or mismatch of the energy bands between the left and the right leads results in the change of the transmission spectra under bias.

With V_b increasing up to 0.4 V, the bands in the left and right lead are shifted downward and upward further, as can be seen from Figure 3g,h. As a result, the doubly degenerate flatband does not match anymore. The matching part of the nondegenerate flatbands becomes very narrow and almost have no contribution to the transmission. Although the match between the nondegenerate flatband and the hybrid band contributes to the transmission,[26] it cannot compensate for the loss of transmission due to mismatch of the flatbands. Consequently, the transmission becomes very small at 0.4 V compared with that at 0.2 V, which is clearly shown in Figure 3i,f. It is worth noting that the magnitude of transmission coefficients is in direct proportion to the group velocity of the matching bands,[27] while

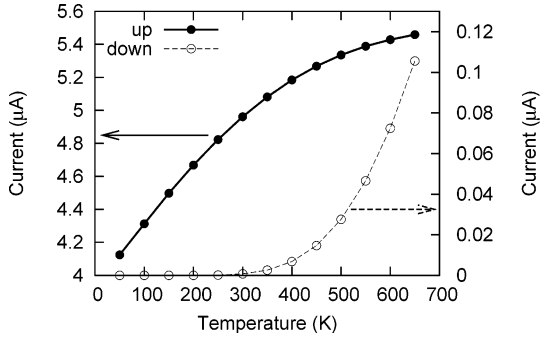

Figure 4. Spin-polarized current as a function of temperature.

the group velocity is proportional to the slope of the band in the form of $v = (1/\hbar)(\partial E/\partial k)$. Therefore, the increase of the transmission from −0.03 eV to 0.35 eV in Figure 3i can be considered to result from the increase of the slope of the matched hybrid band, and the nondegenerate flatband increases in this energy range.

The current $I(V_b)$ can be obtained on the basis of eq 1 from the transmission spectra under various bias voltages. This equation implies that only transmission coefficients in the energy region between μ_l and μ_r contribute to the current integral at zero temperature. Therefore, the energy region between μ_l and μ_r is referred to as the *integral window*, which is indicated by the shaded energy regions in Figure 3f,i. The current−voltage curve in Figure 3a evidently shows that after 0.2 V an apparent NDR behavior, which is characterized by the decrease of the current with the increase of bias voltage, appears for the spin-up current. The appearance of such a NDR phenomenon can be understood through the loss of the transmission due to the mismatch of the bands under increasing bias voltages, as discussed above. For the current at 0.2 V and 0.65 V, the peak-to-valley ratio is 8.9:1. We focus on the positive bias voltages in the above since the current is symmetric with respect to bias polarity because of the symmetric properties of the CNW@SWNT composite. Note that the current for spin-down remains zero at the bias range shown in Figure 3a, since there are no matched bands and therefore no transmission in the integral window. Thus, the current is fully spin-polarized at zero temperature.

Is the current still fully spin-polarized at a finite temperature? At zero temperature, the electron occupation is a step function with the Fermi distribution $f = 1$ below E_F and $f = 0$ above E_F. At a finite temperature, the occupied states near E_F are smeared by the "thermionic emission" effect, and the fraction of electrons with energy above E_F is simply proportional to the Fermi distribution function. We then use eq 2 to calculate the current at a finite temperature. Practically only the transmission in the energy region from a few k_BT below μ_l to a few k_BT above μ_r is needed. Figure 4 shows the evolution of the current as a function of temperature at $V_b = 0.1$ V for CNW@SWNT(8, 0). It apparently shows that both spin-up and spin-down current increase with increasing temperature and that spin-down current becomes significant above 400 K. Thus, at high temperature, the fully spin-polarized current becomes partially spin-polarized, and the extent of the spin polarization decreases. However, in the above discussion, the temperature effect is introduced only as thermal smearing of the Fermi distribution function; other effects such as spin-excitations and phonons are ignored.

In order to probe the effects of different diameters or chiral symmetries of the tube on the degree of spin-polarization for these all-carbon composites, we have also calculated other CNW@SWNT(N, 0) ($N = 9, 7$) and CNW@SWNT(M, M) ($M = 5, 4$) composites. The CNW period is the same as that of the tube for CNWs in zigzag tubes, while it is two times larger than the period of the tube for CNWs in armchair tubes, as used in ref 15. In all of these cases, CNW leads to spin-polarized bands near the Fermi level of the composite. In the case of CNW@SWNT(7, 0), completely spin-polarized bands and transmission appear around E_F, just as the case of CNW@SWNT-(8, 0). In the cases of CNW@SWNT(9, 0), CNW@SWNT(5, 5), and CNW@SWNT(4, 4), only partially spin-polarized transmission appears around E_F. It is known that (5, 5) and (4, 4) tubes are metallic and that there exist bands around E_F for these pure tubes, which are nonspin-polarized; hence, these composites are partially spin-polarized. The pure (9, 0) tube is semiconductive with a very small band gap. However, CNW shifts up the Fermi level of the CNW@SWNT(9, 0) composite and results in the existence of a nonspin-polarized band around E_F from the tube, and therefore, CNW@SWNT(9, 0) is partially spin-polarized.

The effect of a different CNW periodicity on the extent of spin-polarization is further considered. The cases of the CNW period 1 and 1/2 times that of the (5, 5) tube, 1/2 times that of the (8, 0) tube is calculated. Moreover, the dimerization of the CNW in the tube is also investigated. For the case of CNW period 1 times that of the (5, 5) tube (i.e., the interatomic distance of CNW is 2.45 Å), the energy band of the composite is spin-polarized. However, for the case of CNW period 1/2 times that of the (5, 5) tube (with the interatomic distance of about 1.23 Å), the bands for spin-up and spin-down are completely superposed, and then, the composite is nonspin-polarized. For the case of CNW period 1/2 times that of the (8, 0) tube (the interatomic distance is 2.13 Å), spin-polarization of the bands also disappears. The geometry structure of the dimerized CNW in SWNT(8, 0) is taken the same as that in ref 16. Two different dimerization lengths of 1.42 Å and 1.28 Å are considered. From the total energy calculations, we find that the dimerized phase is lower in energy than the undimerized one, and the total energy of the composite is minimized when the dimerization length is 1.42 Å. For the case with the dimerization length of 1.42 Å, the composite is spin-polarized, while it is nonspin-polarized for the case of 1.28 Å. From all of the cases discussed above, we can see that as long as the CNW density is not too high, spin-polarized bands near the Fermi level appear and hence lead to spin-polarized transmission spectra. We note that the magnetism in CNW does not conflict with the Wagner−Mermin theorem,[28] which states that short-range ferromagnetic interaction cannot stabilize a ferromagnetic order in the isolated one-dimensional structures because of gapless spin-excitations. The CNW studied in this work is not an isolated system since it has weak interaction with the SWNT shell, which is the origin of the flatband ferromagnetism of the composite as mentioned at the beginning.

Finally, we also investigate the case of only one carbon atom in the core of the tube, as shown in Figure 1b. For a single carbon atom in the metallic tubes, partially spin-polarized transmission also appears. However, for a single carbon atom in semiconductive tubes, no spin-polarized transmission around E_F appears, since the impurity levels introduced by the carbon atom do not match any band of the pristine tube and therefore have no contribution to the transmission.

4. Conclusion

In conclusion, the spin-polarized transport behavior has been investigated for a kind of all-carbon composites which are composed of CNWs or a single carbon atom in the core of a SWNT. Our results indicate that if the interatomic distance of

CNW is not too small, spin-polarized bands near the Fermi level occur and hence result in spin-polarized transport behavior in such composites. The appearance of NDR can be analyzed from the mismatch of the energy bands in the left and right leads with increasing bias voltages. The results indicate that such a kind of all-carbon composite is a promising candidate for the pure-carbon molecular-spintronic devices.

Acknowledgment. This work was supported by the National Science Foundation of China under Grant 10374091, the special funds for Major State Basic Research Project of China (973) under Grant 2005CB623603, Knowledge Innovation Program of Chinese Academy of Sciences, and Director Grants of Hefei Institutes of Physical Sciences and Institute of Solid State Physics of CAS. Part of the calculations were performed in the Center for Computational Science, Hefei Institutes of Physical Sciences.

References and Notes

(1) Joachim, C.; Gimzewski, J. K.; Aviram, A. *Nature (London)* **2000**, *408*, 541. Heath J. R.; Ratner, M. A. *Phys. Today* **2003**, *56*, 43. Nitzan, A. ; Ratner, M. A. *Science* **2003**, *300*, 1384.

(2) Chen, J.; Reed, M. A.; Rawlett, A. M.; Tour, J. M. *Science* **1999**, *286*, 1550.

(3) Yao, Z.; Postman, H. W. C.; Balents, L.; Dekker, C. *Nature* **1999**, *402*, 273.

(4) Tans, S. J.; Verschueren, A. R. M.; Dekker, C. *Nature* **1998**, *393*, 49. Collier, C. P.; Wong, E. W.; Belohradsky, M.; Raymo, F. M.; Stoddart, J. F.; Kuekes, P. J.; Williams, R. S.; Heath, J. R. *Science* **1999**, *285*, 391. Huang, Y.; Duan, X.; Cui, Y.; Lauhon, L. J.; Kim, K.-H.; Lieber, C. M. *Science* **2001**, *294*, 1313.

(5) Tsukagoshi, K.; Alphenaar, B. W.; Ago, H. *Nature (London)* **1999**, *401*, 572.

(6) Rocha, A. R.; Garcia-Suarez, V. M.; Bailey, S. W.; Lambert, C. J.; Ferrer, J.; Sanvito, S. *Nat. Mater.* **2005**, *4*, 335. Rocha, A. R.; Garcia-Suarez, V. M.; Bailey, S.; Lambert, C.; Ferrer, J.; Sanvito, S. *Phys. Rev. B* **2006**, *73*, 085414. Sanvito, S.; Rocha, A. R. *J. Comp. Theo. Nano.* **2006**, *3*, 624.

(7) Prinz, G. A. *Phys. Today* **1995**, *48*, 58. Prinz, G. A. *Science* **1998**, *282*, 1660. Wolf, S. A.; Awschalom, D. D.; Buhrman, R. A.; Daughton, J. M.; von Molnar, S.; Roukes, M. L.; Chtchelkanova, A. Y.; Treger, D. M. *Science* **2001**, *294*, 1488.

(8) Petta, J. R.; Slater, S. K.; Ralph, D. C. *Phys. Rev. Lett.* **2004**, *93*, 136601.

(9) Xiong, Z. H.; Wu, D.; Vardeny, Z. V.; Shi, J. *Nature (London)* **2004**, *427*, 821; Dediu, V.; Murgia, M.; Matacotta, F. C.; Taliani, C.; Barbanera, S. *Solid State Commun.* **2002**, *122*, 181.

(10) Saito, R.; Dresselhaus, G.; Dresselhaus, M. S. *Physical Properties of Carbon Nanotubes*; Imperial College Press: London, 1998.

(11) Iijima, S. *Nature (London)* **1991**, *354*, 56.

(12) Zhao, B.; Mönch, I.; Mühl, T.; Vinzelberg, H.; Schneider, C. *J. Appl. Phys.* **2002**, *91*, 7026. Zhao, B.; Mönch, I.; Vinzelberg, H.; Mühl, T.; Schneider, C. *Appl. Phys. Lett.* **2002**, *80*, 3144. Sahoo, S.; Kontos, T.; Schönenberger, C.; Sürgers, C. *Appl. Phys. Lett.* **2005**, *86*, 112109. Sahoo, S.; Kontos, T.; Furer, J.; Hoffmann, C.; Gräber, M.; Cottet A.; Schönenberger, C. *Nature Phys.* **2005**, *1*, 99. Hueso, L. E.; Pruneda, J. M.; Ferrari, V.; Burnell, G.; Valdes-Herrera, J. P.; Simons, B. D.; Littlewood, P. B.; Artacho, E.; Mathur, N. D. *Nature* **2007**, *445*, 410. Nagabhirava, B.; Bansal, T.; Sumanasekera, G. U.; Alphenaar, B. W.; Liu, L. *Appl. Phys. Lett.* **2006**, *88*, 023503.

(13) Wang, Z.; Ke, X.; Zhu, Z.; Zhang, F.; Ruan, M.; Yang, J. *Phys. Rev. B* **2000**, *61*, R2472. Zhao, X.; Ando, Y.; Liu, Y.; Jinno, M.; Suzuki, T. *Phys. Rev. Lett.* **2003**, *90*, 187401.

(14) Liu, Y.; Jones, R. O.; Zhao, X.; Ando, Y. *Phys. Rev. B* **2003**, *68*, 125413. Rusznyák, Á.; Zólyomi, V.; Kürti, J.; Yang, S.; Kertesz, M. *Phys. Rev. B* **2005**, *72*, 155420.

(15) Yang, X. P.; Dong, J. M. *Appl. Phys. Lett.* **2005**, *86*, 163105.

(16) Wang, Y.; Huang, Y.; Yang, B.; Liu, R. *Carbon* **2006**, *44*, 456.

(17) Oshiyama, A.; Okada, S.; Saito, S. *Physica B* **2002**, *323*, 21. Choi, J.; Kim, Y. H.; Chang, K. J.; Tománek, D. *Phys. Rev. B* **2003**, *67*, 125421.

(18) Atomistix ToolKit version 2.0, Atomistix A/S (www.atomistix.com). Brandbyge, M.; Mozos, J.-L.; Ordejón, P.; Taylor, J.; Stokbro, K. *Phys. Rev. B* **2002**, *65*, 165401. Soler, J. M.; Artacho, E.; Gale, J. D.; García, A.; Junquera, J.; Ordejón, P.; Sánchez-Portal, D. *J. Phys.: Condens. Matter* **2002**, *14*, 2745. Taylor, J.; Guo, H.; Wang, J. *Phys. Rev. B* **2001**, *63*, 245407.

(19) Datta, S. *Electronic Transport in Mesoscopic Systems*; Cambridge University Press: New York, 1995.

(20) Perdew J. P.; Zunger, A. *Phys. Rev. B* **1981**, *23*, 5048.

(21) Troullier N.; Martins, J. L. *Phys. Rev. B* **1991**, *43*, 1993.

(22) Artacho, E.; Sanchez-Portal, D. Ordejón, P.; Garcia, A.; Soler, J. M. *Phys. Status Solidi B* **1999**, *215*, 809.

(23) Xue Y.; Ratner, M. A. *Phys. Rev. B* **2003**, *68*, 115406.

(24) Blase, X.; Benedict, L. X.; Shirley, E. L.; Louie, S. G. *Phys. Rev. Lett.* **1994**, *72*, 1878.

(25) Farajian, A. A.; Esfarjani, K.; Kawazoe, Y. *Phys. Rev. Lett.* **1999**, *82*, 5084. Leonard, F.; Tersoff, J. *Phys. Rev. Lett.* **2000**, *85*, 4767. Kaun, C.-C.; Larade, B.; Mehrez, H.; Taylor, J.; Guo, H. *Phys. Rev. B* **2002**, *65*, 205416. Stokbro, K.; Taylor, J.; Brandbyge, M.; Mozos, J.-L.; Ordejón, P. *Computational Materials Science* **2003**, *27*, 151.

(26) Note that only the nondegenerate flatband can match with the "hybrid band" because the doubly degenerate flatband has different rotation symmetry with the "hybrid band". This is also identified from the transmission eigenchannel analysis, which shows that only one channel contributes to the transmission, meaning that the doubly degenerate flatband has no contribution to the transmission at 0.4 V .

(27) Fisher D. S.; Lee, P. A. *Phys. Rev. B* **1981**, *23*, 6851.

(28) Mermin N. D.; Wagner, H. *Phys. Rev. Lett.* **1966**, *17*, 1133.